Switch from Conventional to Distributed Kinetics in the Bacteriorhodopsin Photocycle[†]

Andrei K. Dioumaev* and Janos K. Lanyi

Department of Physiology and Biophysics, University of California, Irvine, California 92697-4560

Received July 2, 2008; Revised Manuscript Received August 11, 2008

ABSTRACT: Below 195 K, the bacteriorhodopsin photocycle could not be adequately described with exponential kinetics [Dioumaev, A. K., and Lanyi, J. K. (2007) *Proc. Natl. Acad. Sci. U.S.A. 104*, 9621−9626] but required distributed kinetics, previously found in hemoglobin and myoglobin at temperatures below the vitrification point of the surrounding solvent. The aim of this study is to determine which factors cause the switch from this low-temperature regime to the conventional kinetics observed at ambient temperature. The photocycle was monitored by time-resolved FTIR between 180 and 280 K, using the D96N mutant. Depending on the temperature, decay and temporal redistribution of two or three intermediates (L, M, and N) were observed. Above ∼245 K, an abrupt change in the kinetic behavior of the photocycle takes place. It does not affect the intermediates present but greatly accelerates their decay. Below ∼240 K, a kinetic pattern with partial decay that cannot be explained by conventional kinetics, but suggesting distributed kinetics, was dominant, while above ∼250 K, there were no significant deviations from exponential behavior. The ∼245 K critical point is ≥10 K below the freezing point of interbilayer water, and we were unable to correlate it with any FTIR-detectable transition of the lipids. Therefore, we attribute the change from distributed to conventional kinetics to a thermodynamic phase transition in the protein. Most probably, it is related to the freezing and thawing of internal fluctuations of the protein, known as the dynamic phase transition, although in bacteriorhodopsin the latter is usually believed to take place at least 15 K below the observed critical temperature of ∼245 K.

Bacteriorhodopsin is a small heptahelical protein in the purple membrane of *Halobacterium salinarum* that converts solar energy into transmembrane potential for protons utilized by the living cell (see ref *1* for a recent review). The entire process, from absorption of a photon to the creation of a proton gradient across the membrane, takes place in this protein that undergoes a light-triggered reaction cycle (the "photocycle"), which could be represented in a simplified form as a sequence of spectrally distinct intermediates (bR[1] → K ↔ L ↔ M_1 → M_2 ↔ N ↔ O → bR). During the photocycle, a proton is transported across the membrane, utilizing a complex net of donor and acceptor groups with transiently changing proton affinities. The combination of site-directed mutagenesis and infrared (IR) spectroscopy allowed identification of these groups as carboxylic amino acids (see ref *2* for a review), specifically Asp-85 as the proton acceptor (during the L-to-M transition) and Asp-96 as the proton donor (during the M-to-N transition) to the retinal Schiff base. In the D96N-based family of mutants, the proton is provided from the cytoplasmic side by passive transport with a rate that strongly depends on pH (*3*). This impedes M decay (*3*) and, for purely kinetic reasons, prevents accumulation of the O state and strongly affects the N state kinetics and accumulation.

Spectroscopic studies of the photocycle of bacteriorhodopsin, independent of the particular measuring technique, fall in one of two main categories: (i) time-resolved methods at quasi-ambient temperature (see, for example, refs *4–9*) and (ii) static methods applied to cryogenically trapped states (see refs *10* and *11* for reviews). These two approaches produce similar but not completely identical results (*6*, *12*). Several attempts have been made to bridge the two approaches and to take measurements in the time-resolved mode at low temperatures (*13–17*).

Under ambient conditions, the apparent kinetics of the photocycle can be phenomenologically described with exponentials (*4, 5*) and does not show significant deviation from conventional (exponential) kinetics, although the possibility of a description more complex than distinct exponentials was discussed (*18, 19*). However, when the interconversions of K and L were studied with time-resolved FTIR at 125−195 K, we found that, unlike under ambient conditions, the photocycle dynamics could not be described by distinct exponentials that would imply distinct Arrhenius barriers, and conventional kinetic models led to unresolvable contradictions (*17*). Rather, the photocycle under these conditions required distributed barriers (*17*), in accord with the prediction from studies of hemoglobin and myoglobin

[†] This work was supported in part by grants to J.K.L. from the National Institutes of Health (R01-GM29498) and the U.S. Department of Energy (DEFG03-86ER13525).

* To whom correspondence should be addressed: Department of Physiology and Biophysics, University of California, D340 Med. Sci. I, Irvine, CA 92697-4560. Phone: (949) 824-7783. Fax: (949) 824-8540. E-mail: dioumaev@uci.edu.

[1] Abbreviations: HEPES, *N*-(2-hydroxyethyl)piperazine-*N*′-2-ethanesulfonic acid; CAPS, 3-(cyclohexylamino)-1-propanesulfonic acid; bR, bacteriorhodopsin; K, L, M_1, M_2, N, and O, intermediates of the bacteriorhodopsin photocycle; SVD, singular-value decomposition.

10.1021/bi801247e CCC: $40.75
Published on Web 09/27/2008

that this is a universal feature of protein reactions at low temperatures (*20, 21*). Thus, the dynamics of these systems is qualitatively different at low and ambient temperatures, and this raised the possibility that there might be a critical temperature between 195 K and ambient where one kind of kinetics is switched to the other.

In hemoglobin and myoglobin, two soluble proteins which have been studied in greatest detail (*20, 21*), the distributed kinetics appeared to be the consequence of the freezing of the protein at temperatures below the glass transition of the surrounding solvent (*21, 22*), and this domineering influence of the environment over the dynamic behavior of the protein was called "slaving" (*23*). However, bacteriorhodopsin is an integral membrane protein, and it is neither as exposed to nor as influenced by (*24*) the surrounding solvent as soluble proteins (*21, 22*).

Distributed kinetics is a consequence of the freezing of an ensemble of substates of the protein, which are unable to freely convert (to "thermolize") on the time scale of the spontaneous processes being studied (*20, 21*). The corresponding temperature-induced change in the pattern of internal fluctuations, which is observed in hemoglobin, myoglobin, and bacteriorhodopsin (see refs *21*, *25*, and *26*, respectively, for reviews), is usually termed the "dynamic phase transition". In bacteriorhodopsin, it occurs at or below 230 K (*24*−*31*). However, unlike in the soluble proteins where the dynamic phase transition reflects the glass transition in the surrounding solvent (*23*), the ≤230 K temperature point in bacteriorhodopsin was not correlated with any critical temperature in either water or lipid, the only two components of samples besides bacteriorhodopsin, and therefore, in this system the dynamic phase transition is attributed to freezing and thawing of the protein.

Here we report on further experiments on bacteriorhodopsin and its mutants in the temperature range of 180−280 K. We monitored the kinetic behavior of the photocycle at increasing temperatures, with the aim of determining when, why, and how the relaxation dynamics of the photocycle is converted from distributed kinetics to a process with conventional exponential components. We found that this happens in a very narrow temperature range, like a thermodynamic phase transition, with a midpoint at ∼245 K. Since we were not able to correlate this abrupt change with a process involving either water or lipid, we attribute it to the protein.

MATERIALS AND METHODS

Bacteriorhodopsin and its D96N and D96N/D115N mutants were produced and isolated by a standard procedure (*32*). Purple membranes were deposited on CaF_2 IR windows (Harrick, Ossining, NY) from concentrated suspensions (in 1 mM buffer, HEPES or CAPS, at the desired pH) and dried to approximately room humidity. The samples were rehumidified by placing a 2 μL drop of H_2O close to the purple membrane film and then covered with a second CaF_2 window, separated from the first by a 0.8 mm Teflon spacer. The two windows were sealed by squeezing the Teflon spacer. The sample was allowed to re-equilibrate with water vapor for 48 h before the measurements. After this time, the water content of the sample was constant on the time scale of several weeks and survived repeated cooling−heating cycles.

IR measurements were performed on an IFS-66/s FTIR spectrometer (Bruker) at 2 cm^{-1} resolution for the 0−5250 cm^{-1} spectral range. All measurements were taken in an Optistat DN cryostat equipped with an ITC 601 temperature controller (both by Oxford Instruments, Abingdon, U.K.). An equilibration time of ∼90 min was allowed after each temperature change. Further details about the measurements can be found in ref *17*. Prior to any measurements, the samples were light-adapted at 280 K for 20 min with an arc lamp equipped with a 500 ± 20 nm filter.

For the faster measurements in the 240−280 K temperature range, we employed single-flash excitation with a frequency-doubled Nd:YAG laser (10 ns, 532 nm, ∼2 mJ/cm^2) using rapid scan measurements with a scan rate of 240 kHz and repeated excitation for further averaging. However, even at 280 K, the sample (D96N at pH 6.9) cannot be flashed more frequently than once in ∼30 s, restricting our ability to average, and the acceptable level of the S/N ratio effectively reduced the time resolution to ∼1 s in this series.

For the slower measurements in the 180−240 K temperature range, photoexcitation was provided either by laser flashes as for the measurements at >240 K (see above) or by illumination with an arc lamp (typically for 20 min) equipped with a high-pass filter (>640 nm) that minimizes the probability of secondary photochemistry. The slow dynamics made averaging by repeated excitation impractical below 240 K, and intermediates after the end of illumination were measured from a single excitation in the rapid scan mode at a slower scan rate of 40 kHz.

Kinetics of the spectral changes were monitored for 12 h after either laser flash or the end of continuous light in the rapid-scan mode. The time range was subdivided into 130 time intervals on a quasi-logarithmic time scale. The FTIR spectrometer scans were co-added separately for each time interval with the number of averaged scans doubled after each 10 subsequent time intervals. Signal-to-noise considerations effectively limited the time resolution to 10 s in the data series ≥250 K, reducing it to ∼1 min below this temperature.

We estimate that the light flux from the lamp provides photoinduced conversions with the following rates: $k_{bR\rightarrow K}$ ∼ 1/20 s^{-1} and $k_{K\rightarrow bR}$ ∼ 1/2 s^{-1} (*33*) [which are more rapid than the rate of the K-to-L transition at ≤240 K (see more below)]. In the case of laser excitation, the flash energy was kept low, at ∼2 mJ/cm^2, to prevent photodamage.

To improve the signal-to-noise ratio, the data array was subjected to singular-value decomposition (*34, 35*). Statistical tests on singular values, residuals, and autocorrelations along the time coordinate (see ref *36* for details) revealed that depending on the temperature the observed absorption changes in mid-IR could be ascribed to the presence of two or three spectrally distinct species, i.e., two or three nonrandom basis spectra, indicating the presence of the two or three spectrally distinct intermediates. The rest of the SVD basis spectra originated primarily from stochastic noise (*34, 35*). We retained the two or three nonstochastic basis spectra and one or two additional (primarily noise) basis spectra to ensure the absence of a SVD-induced bias to SVD filter the data. These three to five basis spectra were further routinely corrected for water vapor variations and small baseline distortions that were inevitable when IR spectra were monitored on the time scale of many hours.

When feasible (see Results and Discussion), the kinetics of the photocycle was analyzed by global fitting (*36*); when not feasible, we used the ethylenic stretch depletion recovery for a less rigorous description of the overall recovery rate of the photocycle. Formation of the L, M, and N states is accompanied by this strong negative band, at ~1526 cm^{-1}, from the depletion of the ground state. The amplitudes of the negative ethylenic bands in the differential FTIR spectra of L, M, and N are not too different (*11*), and we could use their kinetics as a convenient measure of the ground state recovery.

Alternatively, qualitatively correct spectra of the intermediates could be calculated from the measured spectra, utilizing known features of their IR spectra (*11*): (i) the lack of the positive Asp-85 band at 1761 cm^{-1} and (ii) the strong positive band at 1400 cm^{-1} in L, (iii) the shift of the Asp-85 band from 1761 to 1753 cm^{-1} during formation of the N state, and distinct differences among the L, M, and N states in (iv) the amide, (v) ethylenic, and (vi) fingerprint regions. From the measured spectra (and their changes) during the illumination at different temperatures, we constructed individual L, M, and N spectra, which contain most probably less than 10% contamination by the two other states. These spectra were further used for evaluation of kinetics of the intermediates. In matrix notation, the measured time-resolved spectral changes, $\Delta A(\nu,t)$, could be represented as a product of two matrices, that of the spectra of intermediates, *spectra*(ν,*i*), and their kinetics, *kinetics*(*i*,*t*) (where *i* values of 1, 2, and 3 correspond to L, M, and N states, respectively):

$$||\Delta A(\nu, t)|| = ||spectra(\nu, i)|| \cdot ||kinetics(i, t)||$$

Using the intermediate spectra, we calculate the best-matching kinetics for individual intermediates:

$$||kinetics(i, t)|| = \text{pseudoinverse}[||spectra(\nu, i)||] \cdot ||\Delta A(\nu, t)||$$

where the pseudoinverse is a mathematical procedure, which allows us to obtain an equivalent [in a least-squares sense, by solving a mathematically overdetermined system of linear equations (*35*)] for the inverse of a nonsquare matrix: pseudoinverse[$||M||$] = $(M^{T} \cdot M)^{-1} \cdot M^{T}$, where $M^{T}$and $(\{\})^{-1}$ are the matrix transpose and matrix inverse, respectively.

OPUS (Bruker), *GRAMS* (Galactic Industries Corp., Salem, NH), *Matlab* (The MathWorks Inc., Natick, MA), *CurveExpert* (http://www.ebicom.net/~dhyams/cmain.htm), and *Fitexp* (*36*) were used for data handling and evaluation.

RESULTS AND DISCUSSION

Photocycle Kinetics in the 180−240 K Range. Within the first minute of continuous illumination (≥640 nm), an equilibrium between the bR and the K states is established, which is strongly shifted toward bR, and the photocycle reactions that follow are due to the relatively small leakage from K to L. However, because the L-to-bR photoreaction is negligible under >640 nm illumination, on the time scale of tens of minutes (depending on temperature) a nearly 100% conversion of bR to the photocycle intermediates takes place.

By the end of the illumination, a mixture of intermediates is created, which is quasi-stable during the first minutes at ≤240 K, and their relative contributions are fully determined by the temperature for constant illumination conditions, in full analogy with the way the time delay determines the observed mixtures in time-resolved experiments at ambient temperature. The spectra measured at the end of the illumination are presented in Figure 1. On the lower end of the measured temperature range (≤200 K), the dominant presence of the L state is evident. At ≥200 K, the rate of the L-to-M reaction accelerates into the time scale of tens of minutes, and increasing amounts of M are formed during illumination. At ≥240 K, a substantial amount of the N state becomes evident due to acceleration of the M-to-N transition.

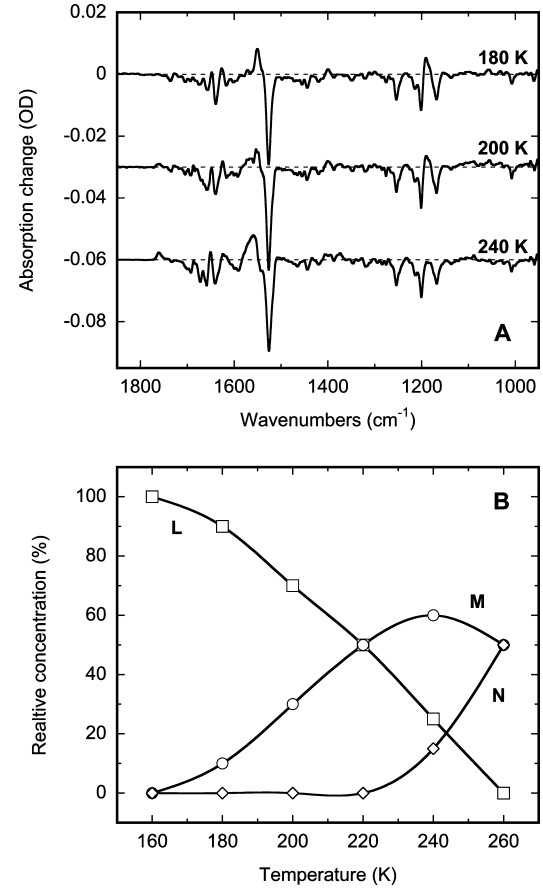

FIGURE 1: (A) Light-induced spectral changes in the D96N mutant (at pH 6.9) by the end of illumination with >640 nm light at 180, 220, and 240 K (cross-scaled by the depletion band of the all-*trans*-retinal at 1254 cm^{-1}). (B) Estimated percentage of L, M, and N intermediates in the mixture formed by the end of the illumination. With less humidified samples, these percentages are humidity-dependent (not shown).

The presence of complex mixtures of intermediates becomes even more evident when their time evolution is monitored on the time scale from ~1 min to hundreds of minutes after the illumination. Not only the initial composition of the intermediates (Figure 1) but also their subsequent thermal redistribution is changed at different temperatures. Figure 2 presents the dynamics of the spectral changes: the measured spectral changes (in panel A) and the normalized spectra (in panel B) at an early (~1 min) versus late time (~300 min) to highlight the corresponding redistribution. The calculated individual kinetics for the L, M, and N intermediates are presented in Figure 3.

Even though our choice of constant illumination at >640 nm should not be expected to produce a significant contribution from secondary photochemistry from re-excitation of the L, M, or N state, minor contamination could not be ruled out. To check for this, we repeated the experiments with

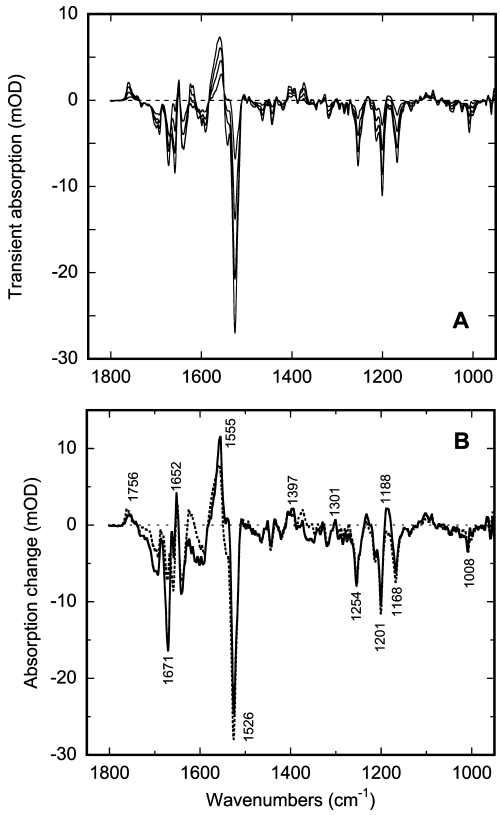

FIGURE 2: Transient spectral changes in the dark of the D96N mutant at pH 6.9 and 240 K. (A) Selected spectra at 1, 10, 50, and 240 min. (B) Spectra obtained from data measured at 240 K by interpolation to times "zero" (broken line) and "infinity" (solid line), with the latter normalized to the former (×3.9) to account for the decay. Spectral decomposition revealed that both the early and late spectra contain contributions from L, M, and N intermediates. The relative contribution of L is nearly unaffected by the decay and accounts for ~25% in both spectra, while the concentration ratio of M to N changes from ~4:1 to ~3:2 from the early to the late spectrum, respectively.

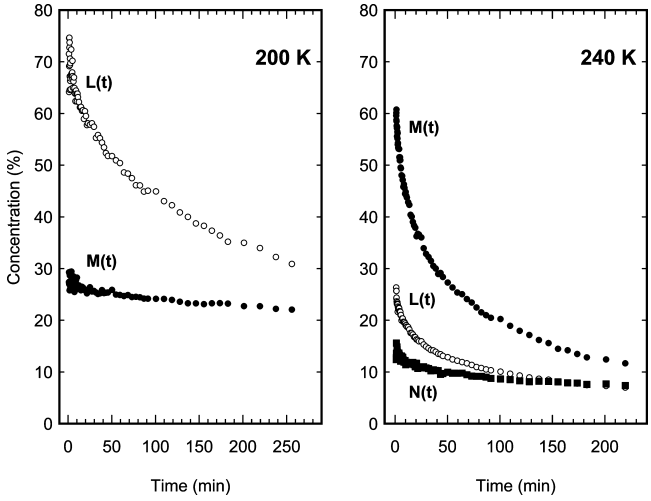

FIGURE 3: Calculated decay kinetics of the L, M, and N intermediates at 200 and 240 K.

single-flash excitation with a 10 ns laser at 523 nm. Unlike excitation with continuous light where nearly 100% conversion is feasible, the short laser flash produced conversion of only ~15% (*33*), restricted by both the efficient K-to-BR photoreaction and the need to use low intensities to prevent photodamage. This led to an ~6−7 times lower S/N ratio, making these data sets inferior to those measured with lamp excitation. Other than this difference, the two data sets were indistinguishable within experimental error, and therefore, the lamp-excited data sets seem to be virtually free of artifacts from double photoexcitation.

Evidence for Distributed Kinetics below 240 K. Despite the spectral and kinetic variations in the time courses at different temperatures (Figures 2 and 3), in the 180−240 K range two important features are in common for all measurements. The first is the presence of a general decay process (see Figures 2A and 3) both at low temperatures, where only the L and M states are present (i.e., no N produced), and at the high end of the temperature range (e.g., at 240 K), where substantial amounts of the N state are also formed.

The second common feature of photocycle dynamics throughout the 180−240 K temperature range is the presence of an apparent end product (Figures 2 and 3), i.e., as if only a portion of each intermediate population (be it the L, M, or N state) undergoes decay while the rest appears stable on the time scale of hundreds of minutes. The molecular composition of this end product depends drastically on temperature, ranging from mostly (>85%) L at 180 K to large amounts (~55%) of M at 220 K and to significant amounts (~30%) of N at 240 K, but the pattern of seemingly unfinished decay persists. For any particular intermediate (L, M, or N), such a pattern might be explained by two kinetically distinct but spectrally similar substates connected by a unidirectional transition (e.g., L_1-to-L_2) and in such a way that only the first but not the second of the two substates undergoes decay, leaving the second state in a kinetic cul-de-sac. However, for this pattern to persist over a wide temperature range (180−240 K) and affect similarly all three different intermediates (L, M, and N), one would have to assume that each of these intermediate has a spectrally similar cousin state in a separate cul-de-sac. An attempt to construct such a kinetic scheme for the low-temperature photocycle runs into extreme problems, because one needs to reconcile the observed apparent rates with the apparent percentages of all these substates, since their branching ratios should be determined solely by the observed kinetics.

Thus, as we reported before, the apparent partial decay is very difficult to reconcile (see more in ref *17*) with any scheme based on distinct steps of conventional kinetics (over fixed Arrhenius-like barriers). Conversely, it is a kinetic signature of distributed kinetics (*17*), which appears when the potential barrier along the reaction coordinate is a distribution around the mean over an ensemble of frozen substates (*21*).

Mathematically, distributed kinetics can be viewed as a limiting case of a fit with an infinite number of exponentials. As a consequence, it can be difficult to distinguish distributed from discrete kinetics, especially when (i) the process is not a single transition and (ii) the dynamic range of the measurements is limited in both time and amplitude, as is in the case of L-to-M-to-N transitions in the 180−240 K range. However, if a multiexponential fit is forced on a data set of a truly distributed kinetics, two kinds of inconsistencies are to be expected. First, distributed kinetics should be possible to represent with sufficient accuracy in a limited time range by a limited sum of exponentials, but any noninfinite number of exponentials would produce an accurate fit for only part of the whole amplitude of the kinetics,

with more and more exponentials required as the dynamic range of measurements is increased. Thus, the presence of an unexpected apparent end product, not warranted by other considerations, is a strong indication of potential deviations from exponential kinetics. The second inconsistency would be that irrespective of the number of exponentials needed, the obtained exponentials differ in their apparent time constants but share the same spectrum; i.e., the components are kinetically distinct but spectrally similar. This is in stark contrast with the multiexponential fits of truly conventional kinetics, e.g., the photocycle at ambient temperatures, in which the spectra (eigenvectors) for different exponentials (eigenvalues) are different. In complex but conventional kinetics, spectrum-oriented SVD analysis and kinetic-oriented analysis based on global multiexponential fits produce comparable estimates for the number of kinetic and spectral components (see ref *36* for more details). In distributed kinetics, however, the number of statistically valid SVD components is far smaller than the number of apparent kinetic components (*17*). These inconsistencies could be used to detect cases in which even in purely kinetic terms the observed dynamics begins to deviate from the conventional (exponential) kinetics.

Both features are strongly present in the kinetic data at ≤240 K. While not a mathematically rigorous direct proof of distributed kinetics, these features indicate sufficiently strong deviation from the conventional (exponential) kinetic pattern. Therefore, we believe that, together with our earlier data on perturbation experiments at still lower temperatures (*17*), we have strong, although indirect, evidence that distributed kinetics is a better description of the data in the 180−240 K range.

Temperature Dependence of the Kinetics between 180 and 240 K. Distributed kinetics cannot be represented by a specific numeric value analogous to the time constant of conventional exponential kinetics, but because its time course in a log−log representation is nearly linear, an estimate of an effective half-time for the corresponding decay can be made. A temperature dependence of such half-times, though lacking the theoretical basis of Arrhenius−Eyring plots, provides a generally correct description of the temperature-induced trend. When the decay data from the 180−240 K range was reduced to an Arrhenius-like plot for these effective half-times, it was linear for the 60 K range, but its extrapolation to 300 K predicted a half-time of ∼7 min (at pH 6.9; see Figure 7). This prediction is in contradiction with the measurements: at ≥260 K the cycle was too rapid to detect with the ∼1 min effective time resolution in our lamp excitation experiments (data not shown). To explore this discrepancy at an increased time resolution, all experiments above 240 K, as shown below, were performed with repetitive excitation by short laser pulses.

Photocycle Kinetics in the 240−280 K Range. Several features, besides the much more rapid rates, distinguish the temperature range above 250 K from that below 240 K (the 240−250 K range being a transition region). The most evident one is that above ∼250 K the photocycle goes to virtual completion without forming apparent end products. Statistical tests on both SVD and global multiexponential fitting (see ref *36* for details) consistently favored the presence of two distinct components in both spectra (from SVD) and kinetics (from global multiexponential fitting). The

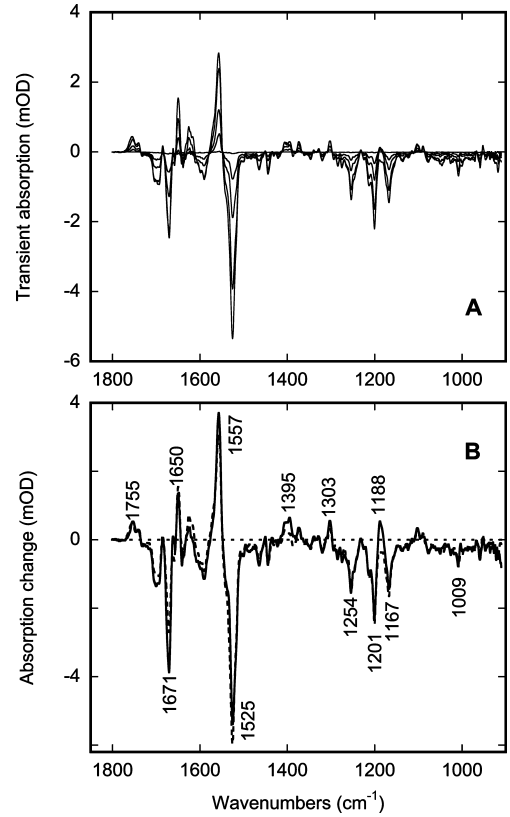

FIGURE 4: Transient spectral changes in the D96N mutant at pH 6.9 and 260 K. Selected spectra at 1, 5, 20, 50, and 200 s (A). (B) Spectral decomposition based on a multiexponential fit (two processes with values of 5.0 ± 0.5 and 31 ± 2 s). The early spectrum (broken line) contains M and N states at an approximately 50:50 ratio, but this ratio is changed in the late spectrum (solid line) to approximately 30:70.

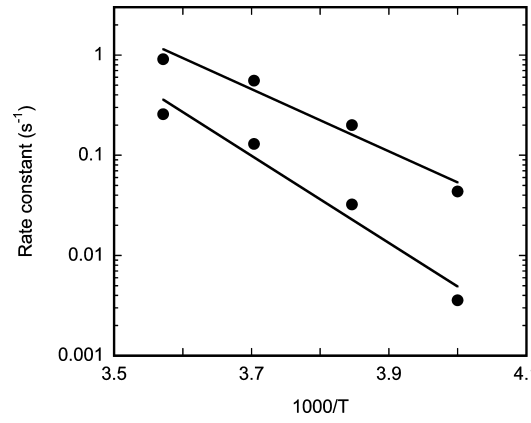

FIGURE 5: Arrhenius plot for the two-exponential approximation of the photocycle kinetics above 250 K. The absence of a strong difference in the temperature dependence of both rate constants leads to the qualitatively similar redistribution of intermediates for the region of 250−280 K and allowed use of the "apparent half-time" estimates in Figure 7.

dynamics of the mid-IR spectra in the 250−280 K range give no indication of deviation from exponential kinetics, in accord with data previously reported by many laboratories under ambient conditions.

The two main intermediates, the M and N states, are present in the spectra at >250 K, and a characteristic spectral evolution (at 260 K) is presented in Figure 4A. Figure 4B presents renormalized spectra calculated from fits by extrapolation to the time before both kinetic components, and

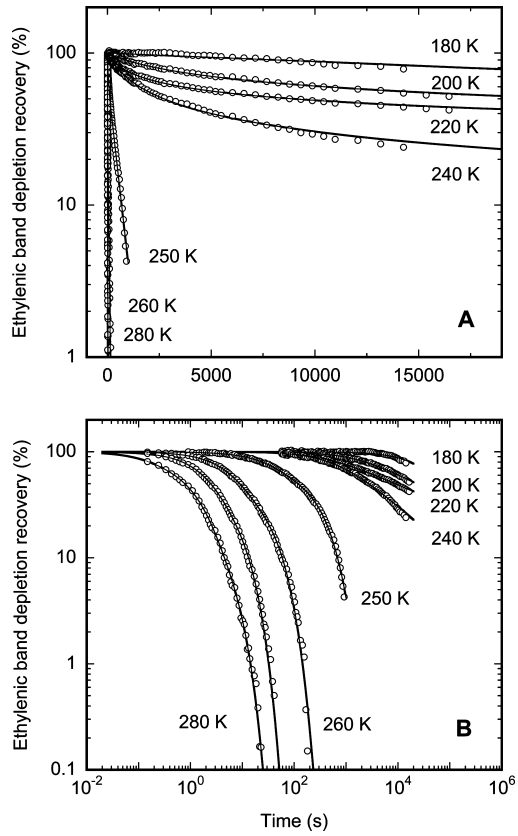

FIGURE 6: Kinetics of the ethylenic stretch depletion band recovery, at 1526 cm^{-1}, in the 180−280 K temperature range, as a qualitative measure of the completion of the photocycle: (A) linear and (B) logarithmic time scales. Note the striking temperature-induced change: above 240 K the photocycle is not only much faster but also completed rather than forming apparent end mixtures as at ≤240 K.

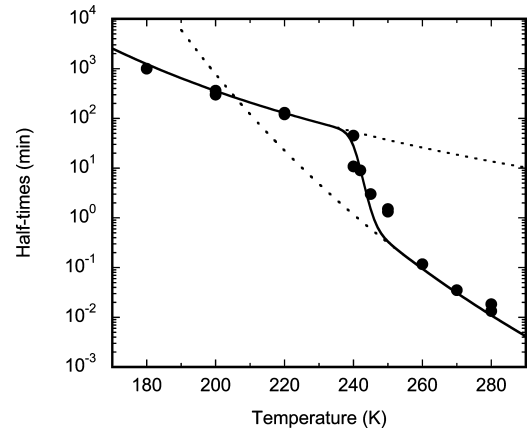

FIGURE 7: Temperature dependence of the apparent half-time of the photocycle completion over the 180−280 K range. The filled circles are the values obtained from the curves like those in Figure 6, and the solid line is a fit with two Arrhenius-like curves with the following values: $\Delta H_1^{\#} = 17 \pm 1$ kJ/mol at ≤240 K and $\Delta H_2^{\#} = 63 \pm 1$ kJ/mol at ≥260 K [the latter being in accord with the ambient temperature data (*4, 5*), and a transition between them centered at ∼245 K]. The dotted lines are the corresponding Arrhenius dependencies for the two separate segments (180−240 and 260−280 K).

that between the two processes as if the first kinetic component were finished and the second has not yet started. Figure 5 presents the temperature dependence of the two apparent kinetic components. Note that the corresponding Eyring enthalpy barriers have comparable values for these two kinetic components, resulting in qualitatively similar observed kinetics at any temperature in the 250−280 K range, where, to a first approximation, only the absolute rate but not the general pattern is affected. Further, this similarity of the enthalpy barriers for the two exponentials (Figure 5) allows qualitative description of the data at >240 K with single half-times (see below).

A Temperature-Induced Switch from Distributed to Conventional Kinetics. Figure 6 presents kinetic traces of the recovery of the bR state, as monitored with ethylenic stretch dynamics, for different temperatures in the 180−280 K range. The solid curves are the results of fits with either two exponentials for the 250−280 K range or a power law for the 180−240 K range (as proposed in ref *37* and applied to bR kinetics at ≤195 K in ref *17*). The most evident feature in the kinetic pattern of behavior is the abrupt change with the onset just above 240 K. It takes place in a very narrow temperature range (Figure 6), and the steepness of the change exceeds by far that of any know temperature-induced change in the bR photocycle.

There is no adequate method for rigorously comparing the temperature dependencies of distributed and multiexponential kinetics. We have chosen to use phenomenological half-times to illustrate the temperature dependence in Figure 7. This presentation correctly demonstrates the presence of a transition, evident also from the change in the kinetic pattern in Figure 6A. Alternatively, one could compare the temperature-induced overall acceleration of the rates between 220 and 240 K, between 240 and 260 K, and between 260 and 280 K. In the region of transition, the observed acceleration of >100-fold is in contrast with the corresponding temperature effects outside the region where they amount to changes of factors of <10.

The kinetically detectable phase transition in Figure 7 could have been a specific feature of the D96N mutant at the given pH and/or hydration level and, thus, could lack the generality expected of a phase transition. To test this, additional measurements were performed on different samples. Thus, besides the D96N mutant, analogous sets of kinetic measurements were taken with wild-type bR and the D96N/D115N mutant, both at physiological and elevated pH (pH ∼10), using both highly hydrated samples and those with a lower level of water present (∼800 H_2O molecules per bR molecule, which is comparable to the level in samples prepared by incubation at 100% humidity). The specific mixtures of intermediates formed by the end of the illumination and their redistribution during their decay were different in these samples. However, the general pattern, the presence of a seemingly thermostable end product below ∼240 K and the disappearance of this feature above ∼250 K, was the same, indicating that the presence of distributed kinetics is an obligatory feature in bR below ∼245 K.

Thermodynamic Behavior of Water and Lipid in the 180−280 K Range. The purple membrane samples include only three components: (i) bacteriorhodopsin, (ii) the native lipids of the purple membrane, and (iii) water, confined in the interbilayer spaces between the membrane sheets. On the basis of an extinction coefficient of bR of ∼63000 M^{-1} cm^{-1} in the visible range (*38*) and the extinction coefficient of water of ∼100 M^{-1} cm^{-1} at 3404 cm^{-1} (*39*), a typical sample contained nearly 70% of water by volume (∼5 μm

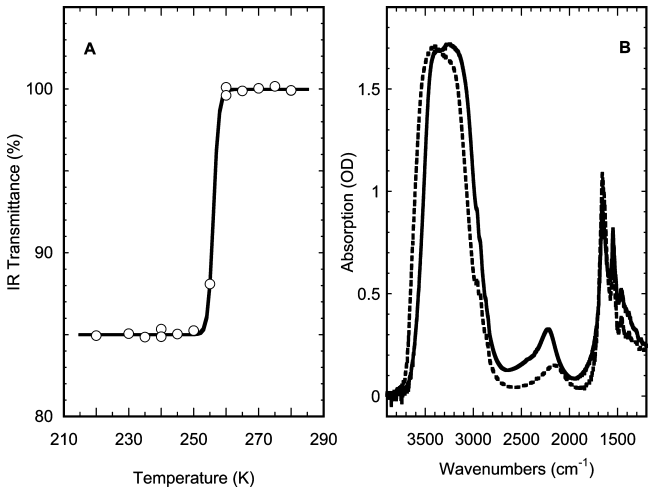

FIGURE 8: IR monitoring of interbilayer water freezing. (A) Temperature dependence of the IR transmittance integrated over the 900−4500 cm^{-1} range, i.e., the raw amplitude of the IR signal measured before Fourier transformation. (B) IR absorption spectra in the two temperature ranges: (i) liquid water at 260−280 K (dashed line with a maximum at ∼3400 cm^{-1}) and (ii) ice at 220−250 K (solid line with a maximum at ∼3200 cm^{-1}). The spectra are virtually indistinguishable within each of these ranges but experience a distinct change at ∼256 K due to freezing of the interbilayer water. Although the IR spectra for the 220−250 K range are slightly different from the spectrum of bulk ice (*42*), the downshift of the whole main water band from ∼3400 to ∼3200 cm^{-1} is typical for freezing (*42*).

of water out of the ∼7.2 μm overall thickness of the film), which corresponds to ∼3200 molecules of water per bR molecule (∼2.2 g of H_2O/g of bR). These values are 4−5-fold higher than those in the samples prepared by prolonged incubation at a relative humidity close to 100% (see, for example, refs *8*, *26*, *28*, *29*, and *40*), and our typical sample has a water to amide I absorption ratio (A_{3400}/A_{1657}) of ∼2.3. This excess of water over the samples prepared by incubation at ∼100% relative humidy is due among other factors to an effective concentration of ∼40 mM buffer, which absorbs water in the excess of that in the case of the low-salt films.

Because of its high concentration, water was the primary suspect as the cause of the transition-like behavior in Figure 7. Confined water is known to freeze well below the freezing point of bulk water at 273 K (e.g., ref *41*). The IR spectrum of ice is different from that of liquid water (*42*), and we used the main water absorption (2900−3800 cm^{-1}) region to monitor the phase state of water in situ from the time-resolved spectra. Figure 8 presents the freezing curve of the interbilayer water. We find that the interbilayer water freezes ∼10 K above the critical point in the temperature dependence of kinetics (Figure 7), i.e., at ∼256 K (Figure 8). The freezing and thawing behavior of interbilayer water is complex (details will be published elsewhere). Water sandwiched between the purple membrane sheets is not homogeneous. When there are 25−30 layers of water in each interbilayer space, as in this report, it is the primary hydration shell, with a width of a few water molecules, that affects bacteriorhodopsin the most, and it might behave differently from the rest of the interbilayer water (*24, 26, 29, 31*). However, these water molecules account for only ∼10% of the IR signal in Figure 8. This limits our ability to detect the specific influence of the primary hydration shell, a question that would be better addressed by using semidried samples. In this work, however, we attempted to study bacteriorhodopsin in its native aqueous environment, with the aim of avoiding dehydration-induced effects.

The second suspect was the lipids. Lipids are polymorphic, and most lipids undergo a "main" phase transition (i.e., freezing of hydrophobic tails) above 250 K (*43*). Earlier calorimetric measurements with purple membranes failed to detect any pronounced thermodynamic transitions in the 240−300 K range (*44*). On the other hand, the main transition in lipids creates a distinct IR signature (*45*), which allows monitoring of their phase state by IR spectroscopy (*45*). Our experiments with pure phosphatidylcholine lipids (to be published separately) indeed revealed distinct shifts in the methyl and methylene bands (2830−2970 cm^{-1} range) by 3−5 cm^{-1}, in accord with earlier reports for other lipids (*45*). In contrast, we found no comparable shifts in the purple membrane films for the entire range of 180−280 K. This lack of a transition might be at least partly due to the dense packing of proteins and lipids in the purple membrane and is consistent with the above-mentioned calorimetric data (*44*). Thus, we were not able to correlate the critical temperature point in the kinetics [at ∼245 K (Figure 7)] with either the freezing of interbilayer water or a detectable phase transition in the lipids.

While the critical point in the kinetics at ∼245 K (Figure 7) is not correlated with the main transition of the lipids, another potential candidate is their glass transition. Normally, the main phase transition in lipids occurs at temperatures (*43*) above the vitrification point (*46, 47*), and the absence of the former, and in fact of any calorimetrically detected transition in purple membranes at >240 K (*44*), argues against a role for lipid vitrification in the measured effects (Figure 7). However, the glass transition in lipids is a poorly studied field, and there are currently no data on vitrification of purple membrane lipids and no clues about the IR signature of lipid vitrification. Therefore, a glass transition in the lipids still might be considered as a distant possible candidate for the cause of the change in the kinetic pattern at ∼245 K.

Correlation with the Dynamic Phase Transition of bR. The critical point in the kinetic pattern of the photocycle reactions (Figure 7) originates most likely from a thermodynamic phase transition in the protein itself. As shown in studies on hemoglobin and myoglobin, the kinetic pattern of the functioning of a protein is closely coupled to the dynamics of its internal fluctuations and the dynamic phase transition defines the turning point, below which the frozen substates dominate and give rise to distributed kinetics (*21*). According to the data we present here, the corresponding change in the kinetic pattern of the photocycle reactions occurs above ∼245 K, while all previous studies on the dynamic phase transition in bR place its critical point at or below 230 K (see, for example, refs *25*, *27−31*, and *48*). How significant is this discrepancy? The change in the kinetic pattern of the photocycle reactions in the 240−250 K region is abrupt (Figures 6 and 7), leaving little room for significant uncertainty in the value of the critical temperature (∼245 K). On the other hand, the critical temperature assigned to the dynamic phase transition in bR (at <230 K) was determined from gradual changes in the temperature dependence of the magnitude of spatial fluctuations (see refs *25* and *48* for reviews). Further, the critical point for the dynamic

phase transition is usually defined as the point of onset of the new pattern of fluctuations (*25*). It is not unreasonable to assume that this new pattern has to develop to some particular extent with increasing temperature to affect the functional dynamics of the membrane protein to the extent seen in Figures 6 and 7. Being a consequence of the changes in the internal dynamics, the change in the relaxation dynamics of the photocycle might occur at temperatures above those of the onset of its cause. Therefore, the observed switch in the kinetic pattern we report here (Figure 7) is most probably a direct consequence of the thawing of internal fluctuations described phenomenologically by the dynamic phase transition.

The Photocycle Events Are Not Affected by the Switch from Distributed to Exponential Kinetics. The decay at <240 K (Figures 2 and 3) seems to be the direct shunt process from L to bR, described in detail in a previous publication (*17*). If so, decay of M (Figures 2 and 3) would most likely imply that, unlike the K-to-L transition that is unidirectional at temperatures below 160 K (*17*), the L-to-M transition becomes reversible at temperatures in the 180−240 K range, as at ambient temperature (*49*). At ≥240 K, the N state appears, and the decay could proceed "backward", through M-to-L-to-bR shunt, as at lower temperatures, or "forward", N-to-bR transition, as at ambient temperature. The details of these alternatives are under study and will be published elsewhere.

The critical temperature point in the kinetics at ∼245 K might have been specific for the photocycle per se, indicating a temperature-controlled step in the progression of intermediates, with a specific transition being allowed above but not below ∼245 K. For example, it has been argued (*26*) that the dynamic phase transition in bR (at ≤230 K) might mark the temperature below which the M_1-to-M_2 transition is blocked and thus the photocycle does not proceed to M_2 or N intermediates. Such a prediction was based on the reasonable argument that liberation of small-scale protein flexibility, marking the unfreezing of the rigid distribution of microscopic conformational substates that leads to distributed kinetics at low temperatures, should be a prerequisite for the large-scale conformational changes associated with the M_1-to-M_2 or M_2-to-N transition. The data in this report provide a surprising contradiction of this plausible idea. The IR spectra of the two M states are very similar (*7, 50*) and would have been difficult to distinguish, but the evident presence of the N state in the photocycle of D96N at neutral pH both below [at 240 K (Figure 2B)] and above [at 260 K (Figure 4B)] the critical transition region indicates that neither the M_1-to-M_2 transition nor the M-to-N transition is coupled to the critical temperature at which the pattern of the kinetics is changed. Thus, it seems that the small-scale and large-scale conformational changes in bacteriorhodopsin are not as correlated as it is often assumed.

In principle, the two patterns of kinetics, the rapid one above ∼250 K and the slow one below ∼240 K (Figure 6), could coexist in kinetic competition with one another over a wider temperature range (200−260 K). Extrapolation of the high-temperature Arrhenius-like curve (the dotted line in Figure 7) to below 240 K indicates that if the two mechanisms were in kinetic competition, the faster one should have won out at all temperatures above the crossing point, i.e., above ∼205 K. In reality, the faster pattern begins to win only at an ∼35 K higher temperature, at >240 K, indicating that there is a switch, which is not based on kinetic competition.

Thus, the observed critical point at ∼245 K is specific not for the appearance or disappearance of particular reactions in the photocycle, but rather for the general kinetic pattern of the individual transitions, which proceed according to different laws (distributed vs Arrhenius-like barriers) in the frame of one unaltered scheme of the photocycle. The correlation of this temperature point with a switch between distributed and conventional kinetics is still somewhat tentative, for we might have missed small deviations from exponentiality in the data above ∼250 K. However, the drastic phenomenological change in the 240−250 K temperature region (Figures 6 and 7) is beyond any doubt.

ACKNOWLEDGMENT

We express our thanks to Jennifer Wang, who grew and isolated the bR and its mutants.

REFERENCES

1. Lanyi, J. K. (2004) Bacteriorhodopsin. *Annu. Rev. Physiol. 66*, 665–688.
2. Dioumaev, A. K. (2001) Infrared methods for monitoring the protonation state of carboxylic amino acids in the photocycle of bacteriorhodopsin. *Biochemistry (Moscow, Russ. Fed.) 66*, 1269–1276.
3. Cao, Y., Váró, G., Chang, M., Ni, B. F., Needleman, R., and Lanyi, J. K. (1991) Water is required for proton transfer from aspartate-96 to the bacteriorhodopsin Schiff base. *Biochemistry 30*, 10972–10979.
4. Xie, A. H., Nagle, J. F., and Lozier, R. H. (1987) Flash spectroscopy of purple membrane. *Biophys. J. 51*, 627–635.
5. Chizhov, I., Chernavskii, D. S., Engelhard, M., Müller, K.-H., Zubov, B. V., and Hess, B. (1996) Spectrally silent transitions in the bacteriorhodopsin photocycle. *Biophys. J. 71*, 2329–2345.
6. Hessling, B., Souvignier, G., and Gerwert, K. (1993) A model-independent approach to assigning bacteriorhodopsin's intramolecular reactions to photocycle intermediates. *Biophys. J. 65*, 1929–1941.
7. Rödig, C., Chizhov, I., Weidlich, O., and Siebert, F. (1999) Time-resolved step-scan Fourier transform infrared spectroscopy reveals differences between early and late M intermediates of bacteriorhodopsin. *Biophys. J. 76*, 2687–2701.
8. Lorenz-Fonfria, V. A., Furutani, Y., and Kandori, H. (2008) Active internal waters in the bacteriorhodopsin photocycle. A comparative study of the L and M intermediates at room and cryogenic temperatures by infrared spectroscopy. *Biochemistry 47*, 4071–4081.
9. Dioumaev, A. K., and Braiman, M. S. (1997) Two bathointermediates in the bacteriorhodopsin photocycle, distinguished by nanosecond time-resolved FTIR spectroscopy. *J. Phys. Chem. B 101*, 1655–1662.
10. Balashov, S. P., and Ebrey, T. G. (2001) Trapping and spectroscopic identification of the photointermediates of bacteriorhodopsin at low temperatures. *Photochem. Photobiol. 73*, 453–462.
11. Maeda, A. (1995) Application of FTIR spectroscopy to the structural study on the function of bacteriorhodopsin. *Isr. J. Chem. 35*, 387–400.
12. Weidlich, O., and Siebert, F. (1993) Time resolved step scan FTIR investigations of the transition from KL to L in the bacteriorhodopsin photocycle. Identification of chromophore twists by assigning hydrogen out of plane (HOOP) bending vibrations. *Appl. Spectrosc. 47*, 1394–1400.
13. Dioumaev, A. K., Chernavskii, D. S., Ormos, P., Váró, G., and Keszthelyi, L. (1992) Kinetics of the fast electric signal from oriented purple membrane. *Biophys. J. 61*, 1194–1200.
14. Dioumaev, A. K., and Keszthelyi, L. (1988) Low temperature restriction of charge shift in the primary reaction of the bacteriorhodopsin photocycle. *Acta Biochim. Biophys. Hung. 23*, 271–278.

15. Ormos, P. (1991) Infrared spectroscopic demonstration of a conformational change in bacteriorhodopsin involved in proton pumping. *Proc. Natl. Acad. Sci. U.S.A. 88*, 473–477.
16. Ormos, P., Chu, K., and Mourant, J. (1992) Infrared study of the L, M, and N intermediates of bacteriorhodopsin using the photoreaction of M. *Biochemistry 31*, 6933–6937.
17. Dioumaev, A. K., and Lanyi, J. K. (2007) Bacteriorhodopsin photocycle at cryogenic temperatures: Kinetics revealed distributed barriers of conformational substates. *Proc. Natl. Acad. Sci. U.S.A. 104*, 9621–9626.
18. Zimányi, L., Cao, Y., Needleman, R., Ottolenghi, M., and Lanyi, J. K. (1993) Pathway of proton uptake in the bacteriorhodopsin photocycle. *Biochemistry 32*, 7669–7678.
19. Lukacs, A., and Papp, E. (2004) Bacteriorhodopsin photocycle kinetics analyzed by the maximum entropy method. *J. Photochem. Photobiol., B 77*, 1–16.
20. Parak, F., and Frauenfelder, H. (1993) Protein dynamics. *Phys. A (Amsterdam, Neth.) 201*, 332–345.
21. Frauenfelder, H., Parak, H., and Young, R. D. (1988) Conformational substates in proteins. *Annu. Rev. Biophys. Biophys. Chem. 17*, 451–479.
22. Iben, I. E. T., Braunstein, D., Doster, W., Frauenfelder, H., Hong, M. K., Johnson, J. B., Luck, S., Ormos, P., Schulte, A., Steinbach, P. J., Xie, A. H., and Young, R. D. (1989) Glassy behavior of a protein. *Phys. Rev. Lett. 62*, 1916–1919.
23. Fenimore, P. W., Frauenfelder, H., McMahon, B. H., and Parak, F. G. (2002) Slaving: Solvent fluctuations dominate protein dynamics and functions. *Proc. Natl. Acad. Sci. U.S.A. 99*, 16047–16051.
24. Wood, K., Plazanet, M., Gabel, F., Kessler, B., Oesterhel, D., Tobias, D. J., Zaccai, G., and Weik, M. (2007) Coupling of protein and hydration-water dynamics in biological membranes. *Proc. Natl. Acad. Sci. U.S.A. 104*, 18049–18054.
25. Gabel, F., Bicout, D., Lehnert, U., Tehei, M., Weik, M., and Zaccai, G. (2002) Protein dynamics studied by neutron scattering. *Q. Rev. Biophys. 35*, 327–367.
26. Buchsteiner, A., Lechner, R. E., Haub, T., and Dencher, N. A. (2007) Relationship between structure, dynamics and function of hydrated purple membrane investigated by neutron scattering and dielectric spectroscopy. *J. Mol. Biol. 371*, 914–923.
27. Parak, F., Fischer, M., Heidemeier, J., Engelhard, M., Kohl, K.-D., Hess, B., and Formanek, H. (1990) Investigation of the dynamics of bacteriorhodopsin. *Hyperfine Interact. 58*, 2381–2385.
28. Ferrand, M., Dianoux, A. J., Petry, W., and Zaccai, G. (1993) Thermal motions and function of bacteriorhodopsin in purple membranes: Effects of temperature and hydration studied by neutron scattering. *Proc. Natl. Acad. Sci. U.S.A. 90*, 9668–9672.
29. Lechner, R. E., Fitter, J., Dencher, N. A., and Hauss, T. (1998) Dehydration of biological membranes by cooling: An investigation on the purple membrane. *J. Mol. Biol. 277*, 593–603.
30. Fitter, J., Lechner, R. E., Büldt, G., and Dencher, N. A. (1996) Internal molecular motions of bacteriorhodopsin: Hydration-induced flexibility studied by quasielastic incoherent neutron scattering using oriented purple membranes. *Proc. Natl. Acad. Sci. U.S.A. 93*, 7600–7605.
31. Fitter, J., Lechner, R. E., and Dencher, N. A. (1999) Interactions of hydration water and biological membranes studied by neutron scattering. *J. Phys. Chem. B 103*, 8036–8050.
32. Oesterhelt, D., and Stoeckenius, W. (1974) Isolation of the cell membrane of *Halobacterium halobium* and its fractionation into red and purple membrane. *Methods Enzymol. 31*, 667–678.
33. Dioumaev, A. K., Savransky, V. V., Tkachenko, N. V., and Chukharev, V. I. (1989) Qunatum yield and extinction measurements in strongly overlapping reactant and photoproduct absorption bands. II: Bathointermediate formation in bacteriorhodopsin photocycle at room temperature. *J. Photochem. Photobiol., B 3*, 397–410.
34. Henry, E. R., and Hofrichter, J. (1992) Singular Value Decomposition: Application to analysis of experimental data. *Methods Enzymol. 210*, 129–192.
35. Golub, G. H., and Van Loan, C. F. (1996) *Matrix computations*, Johns Hopkins University Press, Baltimore.
36. Dioumaev, A. K. (1997) Evaluation of intrinsic chemical kinetics and transient product spectra from time-resolved spectroscopic data. *Biophys. Chem. 67*, 1–25.
37. Austin, R. H., Beeson, K. W., Eisenstein, L., Frauenfelder, H., and Gunsalus, I. C. (1975) Dynamics of ligand-binding to myoglobin. *Biochemistry 14*, 5355–5373.
38. Rehorek, M., and Heyn, M. P. (1979) Binding of all-trans-retinal to the purple membrane. Evidence for cooperativity and determination of the extinction coefficient. *Biochemistry 18*, 4977–4983.
39. Venyaminov, S. Y., and Prendergast, F. G. (1997) Water (H_2O and D_2O) molar absorptivity in the 1000−4000 cm^{-1} range and quantitative infrared spectroscopy of aqueous solutions. *Anal. Biochem. 248*, 234–245.
40. Berntsen, P., Bergman, R., Jansson, H., Weik, M., and Swenson, J. (2005) Dielectric and calorimetric studies of hydrated purple membrane. *Biophys. J. 89*, 3120–3128.
41. Weik, M., Lehnert, U., and Zaccai, G. (2005) Liquid-like water confined in stacks of biological membranes at 200 K and its relation to protein dynamics. *Biophys. J. 89*, 3639–3646.
42. Ewing, G. E., Foster, M., Cantrell, W., and Sadtchenko, V. (2003) Thin film water on insulator surfaces. In *Water in Confining Geometries* (Buch, V., and Devlin, J. P., Eds.) pp 179−211, Springer-Verlag, Berlin.
43. Koynova, R., and Caffrey, M. (1998) Phases and phase transitions of the phosphatidylcholines. *Biochim. Biophys. Acta 1376*, 91–145.
44. Chen, J. S., Barton, P. G., Brown, D., and Kates, M. (1974) Osmometric and microscopic studies on bilayers of polar lipids from extreme halophile *Halobacterium cutirubrum*. *Biochim. Biophys. Acta 352*, 202–217.
45. Casal, H. L., and Mantsch, H. H. (1984) Polymorphic phase-behavior of phospholipid-membranes studied by infrared-spectroscopy. *Biochim. Biophys. Acta 779*, 381–401.
46. Shalaev, E. Y., and Steponkus, P. L. (2001) Phase behavior and glass transition of 1,2-dioleoylphosphatidylethanolamine (DOPE) dehydrated in the presence of sucrose. *Biochim. Biophys. Acta 1514*, 100–116.
47. Blöcher, D., Gutermann, R., Henkel, B., and Ring, K. (1984) Physicochemical characterization of tetraether lipids from *Thermoplasma acidophilum*. Differential scanning calorimetry studies on glycolipids and glycophospholipids. *Biochim. Biophys. Acta 778*, 74–80.
48. Dencher, N. A., Sass, H. J., and Büldt, G. (2000) Water and bacteriorhodopsin: Structure, dynamics, and function. *Biochim. Biophys. Acta 1460*, 192–203.
49. Váró, G., and Lanyi, J. K. (1990) Pathways of the rise and decay of the M photointermediate s of bacteriorhodopsin. *Biochemistry 29*, 2241–2250.
50. Hessling, B., Herbst, J., Rammelsberg, R., and Gerwert, K. (1997) Fourier transform infrared double-flash experiments resolve bacteriorhodopsin's M_1 to M_2 transition. *Biophys. J. 73*, 2071–2080.

BI801247E